PCCP

PAPER

View Article Online
View Journal | View Issue

Cite this: *Phys. Chem. Chem. Phys.*, 2017, **19**, 22691

Indirect dynamics in S_N2@N: insight into the influence of central atoms†

Xu Liu,[a] Chenyang Zhao,[a] Li Yang,[a]* Jiaxu Zhang[a]* and Rui Sun[b]

Received 22nd June 2017,
Accepted 3rd August 2017

DOI: 10.1039/c7cp04199c

rsc.li/pccp

Central atoms have a significant influence on the reaction kinetics and dynamics of nucleophilic substitution (S_N2). Herein, atomistic dynamics of a prototype S_N2@N reaction F^- + NH_2Cl is uncovered employing direct dynamics simulations that show strikingly distinct features from those determined for a S_N2@C congener F^- + CH_3Cl. Indirect scattering is found to prevail, which proceeds predominantly through a hydrogen-bonded F^-–HNHCl complex in the reactant entrance channel. This unexpected finding of a pronounced contribution of indirect reaction dynamics, even at a high collision energy, is in strong contrast to a general evolution from indirect to direct dynamics with enhanced energy that characterizes S_N2@C. This result suggests that the relative importance of different atomic-level mechanisms may depend essentially on the interaction potential of reactive encounters and the coupling between inter- and intramolecular modes of the pre-reaction complex. For F^- + NH_2Cl the proton transfer pathway is less competitive than S_N2. A remarkable finding is that the more favorable energetics for NH_2Cl proton transfer, as compared to that for CH_3Cl, does not manifest itself in the reaction dynamics. The present work sheds light on the underlying reaction dynamics of S_N2@N, which remain largely unclear compared to well-studied S_N2@C.

Introduction

Nucleophilic substitution (S_N2) reactions have attracted extensive attention both experimentally and theoretically due to their rich reaction dynamics and important role in organic and biological chemistry.[1] The traditional mechanism for S_N2 reactions at the carbon center (S_N2@C) features a double-minimum potential energy surface (PES) with a C_{3V} $[X–CH_3–Y]^-$ central barrier separating two ion–dipole X^-–CH_3Y and XCH_3–Y^- complexes.[2] The barrier represents a transition state (TS) corresponding to Walden inversion at the reaction center as described in textbooks, which plays a significant role in the reaction dynamics. Note that a S_N2@C reaction may occur *via* a nontraditional PES that involves hydrogen bonding. For the OH^- anion reacting with CH_3I, the pre-reaction complex becomes a hydrogen-bonded one with OH^- attached to a C–H bond, *i.e.*, OH^-–HCH_2I.[3] For the OH^- + CH_3F reaction there is a deep hydrogen-bonded CH_3OH–F^- potential energy minimum in the product exit channel instead of the conventional $HOCH_3$–F^- complex.[4] Electronic structure calculations for F^- + CH_3Y (Y = Cl and I) show that the pre-reaction PES has a hydrogen-bonded F^-–HCH_2Y complex together with a second close-lying complex of ion–dipole F^-–CH_3Y and they can transform into each other readily.[5,6] Double labeling experiments[7] have inferred the existence of a classical TS for displacement at the nitrogen center (S_N2@N) and from a theoretical point of view,[8,9] the PES profile for S_N2@N resembles the double-well potential model for S_N2@C. However, the complexes involving nitrogen are characterized by a NH–X hydrogen bond, in contrast to their traditional ion–dipole carbon counterparts. There have been extensive studies of S_N2@C reactions in the past few decades[10–14] that largely enriched our fundamental knowledge on substitution dynamics.[15,16] Nonetheless, studies on the dynamics of S_N2@N, which are of great interest and might be much different, are more limited.[17,18] Due to the inefficient intramolecular vibrational energy redistribution (IVR) and extensive central barrier recrossings, the statistical theories such as Rice–Ramsperger–Kassel–Marcus (RRKM) and transition state theory (TST) without further corrections are suggested not qualified to model the reaction kinetics of F^- + NH_2F.[19] In addition, trajectory calculations of the OH^- + CH_3ONO_2 reaction have successfully reproduced the experimental findings in selectivity of substitution (S_N2) *vs* elimination (E2) pathways and addressed the atomistic reaction mechanisms, which failed to be adequately accounted for using a usual statistical approach.[20]

[a] *MIIT Key Laboratory of Critical Materials Technology for New Energy Conversion and Storage, School of Chemistry and Chemical Engineering, Harbin Institute of Technology, Harbin 150001, P. R. China. E-mail: yangli2014@hit.edu.cn, zhjx@hit.edu.cn*

[b] *Department of Chemistry, University of Hawaii at Manoa, Honolulu, HI 96822-2275, USA*

† Electronic supplementary information (ESI) available: Relative contributions of various mechanisms and atomistic snapshots illustrating the dominant direct stripping event for the proton transfer reaction at 40 kcal mol^{-1} collision energy. Product energy partitioning and velocity scattering angle distributions for the F^- + NH_2Cl → NH_2F + Cl^- S_N2 reaction. See DOI: 10.1039/c7cp04199c

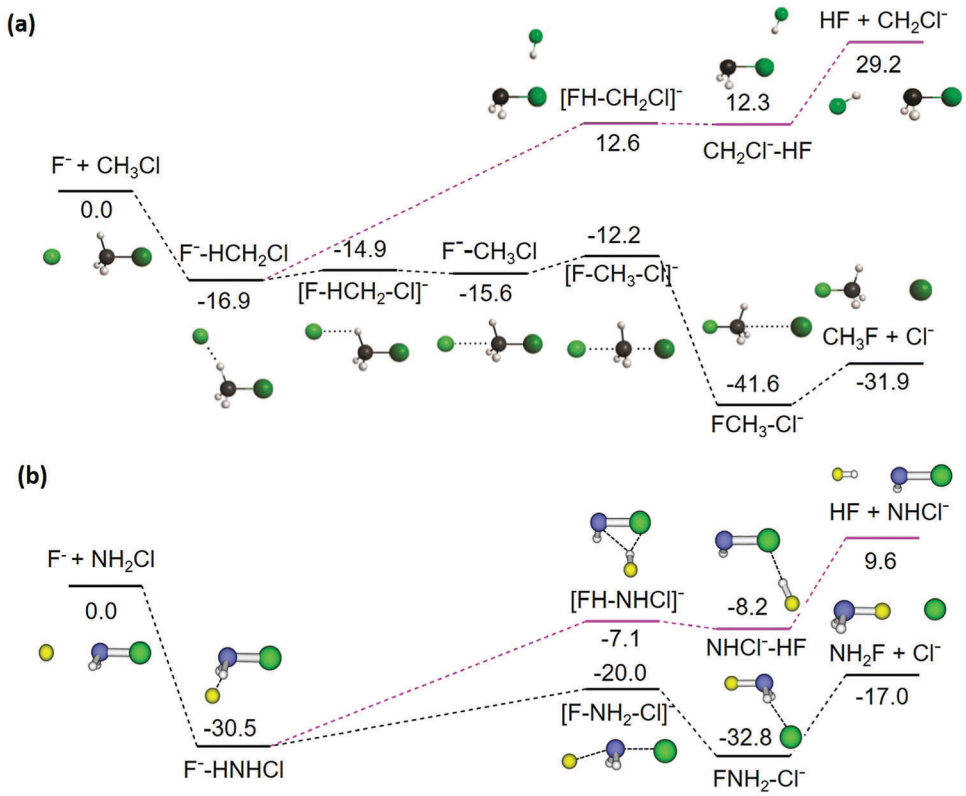

Fig. 1 Schematic representation of the potential energy surface showing the stationary points along S_N2 (black) and proton transfer (pink) pathways for (a) the F^- + CH_3Cl reaction with a focal-point analysis (FPA) method[21] and (b) the F^- + NH_2Cl reaction at the B3LYP/aug-cc-pVDZ level of theory.[23] The numbers indicate classical energies in kcal mol^{-1} without zero-point energy (ZPE).

In view of the large reaction exothermicity and a small central barrier with respect to the reactant complex, the F^- + CH_3Cl → CH_3F + Cl^- S_N2 reaction is of particular interest.[14,16] Its PES, as depicted in Fig. 1(a), deviates somewhat from the double-well potential energy profile that characterizes S_N2@C reactions in the gas-phase.[5,21] Besides the traditional F^-–CH_3Cl ion–dipole complex, a slightly more stable F^-–HCH_2Cl hydrogen-bonded complex is found as a minimum in the entrance channel. Even though the barrier is quite low for them to pass the central barrier and form products, these complexes are predicted from quasi-classical trajectory (QCT) calculations to play an important role in the reaction dynamics and the vast majority of the reactive trajectories at low collision energy proceed through an indirect mechanism with formation of a reaction intermediate in the F^-–HCH_2Cl and F^-–CH_3Cl pre-reaction potential energy well.[5,22] For the present F^- + NH_2Cl reaction, whose stationary atomic configurations are presented in Fig. 1(b),[23] the entrance channel is also characterized by a hydrogen-bonded F^-–HNHCl complex with a similar structure to the carbon analogue. An intriguing question is whether this nitrogen S_N2 reaction features dynamics that bear similarities to the corresponding F^- + CH_3Cl reaction. For the latter, an evolution from indirect to direct dynamics with enhanced collision energy (E_{coll}) has been observed.[21,24] Is this also the case for the NH_2Cl reaction? As shown in Fig. 1, in addition to the S_N2 pathway leading to CH_3F/NH_2F + Cl^- products, the F^- + CH_3Cl/NH_2Cl reaction has a proton transfer (PT) pathway, where the hydrogen-bonded F^-–HCH_2Cl/F^-–HNHCl pre-reaction complex undergoes a concerted H-shift from the C/N to F atom and a migration of HF from the C/N to Cl atom forming a CH_2Cl^-–HF/$NHCl^-$–HF complex with its subsequent fragmentation resulting in the HF and CH_2Cl^-/$NHCl^-$ product species. Despite the fact that the S_N2 channel is generally preferred over the PT channel for both reactions in energy, QCT studies reveal that the F^- + CH_3Cl reactive collisions are governed by the S_N2 mechanism for low E_{coll}, but PT becomes important as E_{coll} increases.[21] The F^- + NH_2Cl reaction has been investigated at room temperature by Bierbaum *et al.* using the flowing afterglow selected ion flow tube (FA-SIFT) technique,[25] and the results indicate that in accordance with the low energy dynamics found for CH_3Cl, nucleophilic substitution at nitrogen yielding NH_2F + Cl^- dominates the NH_2Cl reaction with no PT products observed. However, in going from CH_3Cl to NH_2Cl, the PES shows that the PT pathway becomes energetically more favored irrespective of its retained endoergic feature (Fig. 1). Consequently, an issue of quite interest is how it competes with the S_N2 pathway in the F^- + NH_2Cl system for a higher energy. In experiments, the reaction of NH_2Cl with F^- is found to be approximately twice as reactive as the analogous reaction of CH_3Cl at a thermal energy corresponding to 300 K (E_{coll} ∼ 0.9 kcal mol^{-1}).[25] Does the reaction efficiency depend on the collision energy of reactants? If yes, what inspires one's curiosity is how the range of the

impact parameter b and the value of the opacity function (reaction probability P_r *vs.* b) change when the reactivity varies at a different E_{coll} value. Can the entrance and/or exit channel complexes play a role in the dynamics? How does the energy flow during the course of the reaction and what are the product scattering distributions?

To date, understanding the S_N2 reactions at the nitrogen center has been mainly restricted to identifying the stationary points and minimum-energy pathways (MEPs). This does not allow one to infer the atomistic details of the reaction mechanisms, which can only be uncovered using reaction dynamics simulations.[26,27] In this work, these simulations on the full-dimensional PES are performed to address the above questions, which reveal the underlying dynamics in great detail for S_N2@N. A comparison between the reaction of NH_2Cl with F^- and the corresponding reaction of CH_3Cl further sheds light on the influence of central atoms on the proceedings of nucleophilic substitution and proton transfer reaction dynamics.

Computational procedure

In the present study, we have performed chemical dynamics simulations for the F^- + NH_2Cl reaction following the motion of the atoms along the reaction path using the VENUS dynamics computer program[28,29] interfaced to the NWChem electronic structure computer program.[30] Trajectories are propagated employing a direct dynamics method[31] on the B3LYP/aug-cc-pVDZ PES. This theory has proven successful in establishing an atomic-level understanding of the experiments involving dynamics studies of nucleophilic substitution,[20,32] nonstatistical and nontraditional behaviors,[33,34] and the organic synthesis.[35] Fig. 1 shows that the prominent S_N2 pathway for F^- + NH_2Cl goes through a pre-reaction H-bonded F^-–HNHCl complex, a $[F–NH_2–Cl]^-$ TS, and a post-reaction $FNH_2–Cl^-$ H-bonded minimum to the NH_2F + Cl^- product asymptote. Without zero-point energy (ZPE) included, the B3LYP/aug-cc-pVDZ energies for these stationary points are −30.5, −20.0, −32.8, and −17.0 kcal mol^{-1}, respectively, which are in good agreement with the benchmark CBS-QB3[36] values of −30.7, −17.7, −31.7, and −16.1 kcal mol^{-1} with the largest difference of 2.3 kcal mol^{-1} for the TS $[F–NH_2–Cl]^-$. Results are reported for an average E_{coll} value at 300 K temperature of experiments (E_{coll} ∼ 0.9 kcal mol^{-1})[25] and the reactants' vibrational (v) and rotational (r) degrees of freedom are selected from their 300 K Boltzmann distributions. Note that the PT product reaction channel opens at higher collision energies (Fig. 1), and the dynamics calculations are accordingly carried out with the same v/r temperatures but for a greater E_{coll} value of 40 kcal mol^{-1} to probe the competition between PT and S_N2 reactions, and elucidate the energy dependence of the dynamic features. Similar E_{coll}s were considered for the C-center F^- + CH_3Cl studies as well,[5,21,24] thereby permitting a straightforward comparison of the reaction dynamics between S_N2@C and S_N2@N.

Quasiclassical sampling, which includes ZPE, is used to determine initial coordinates and momenta for the trajectories, as documented elsewhere.[31] Instead of sampling the impact parameter b randomly, the trajectories are calculated at fixed b scanned from 1 Å to the limiting value b_{max} with a step size of 1 and 2 Å for the respective E_{coll} values of 0.9 and 40 kcal mol^{-1}. b_{max} is determined for which there are no reactions out of 100 trajectories and the resulting values are around 12 and 5 Å for the two energies. A total of ∼400 and 700 trajectories are computed at each E_{coll}, respectively.

Results and discussion

Reactivity

The reaction probability P_r as a function of the impact parameter b, *i.e.*, opacity function, is inspected in Fig. 2. The exothermic S_N2 reaction channel F^- + NH_2Cl → NH_2F + Cl^-, which does not have a barrier, is observed at both 300 K (∼0.9 kcal mol^{-1}) and 40 kcal mol^{-1} collision energies, and changing E_{coll} may alter its shape of the opacity function. For collisions at a low E_{coll} value of 0.9 kcal mol^{-1}, the S_N2 reaction probability is high for b = 1, ∼75%, and generally decreases with enhanced b, but P_r falls down essentially to not more than 10% for each b at 40 kcal mol^{-1}. Moreover, the maximum impact parameter (b_{max}) shifts from 12 to 5 Å as E_{coll} increases from 0.9 to 40 kcal mol^{-1}. As a result, the integral cross section (σ), obtained by integrating $P_r(b)$ over the impact parameter $\left(\int P_r(b)2\pi b\mathrm{d}b\right)$, is large at low E_{coll} and drops rapidly with the increase in E_{coll}, and the resulting values are 105.8 ± 10.2 and 5.3 ± 1.3 Å^2, respectively, at 0.9 and 40 kcal mol^{-1}. The negative E_{coll} dependence of σ is understood that the substitution reaction is exothermic without a positive barrier and the longer interaction times and the long-range attractive ion–dipole interactions at lower E_{coll} allow the reactive events even at larger impact parameters. The proton transfer reaction F^- + NH_2Cl → HF + $NHCl^-$ is endothermic and the PT saddle point is well below the product asymptote. With ZPE included, the B3LYP/aug-cc-pVDZ threshold energy is

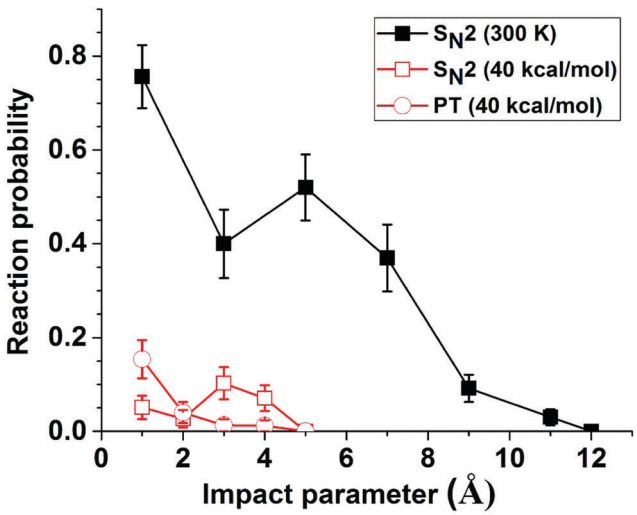

Fig. 2 Opacity functions of the F^- + NH_2Cl reaction for the substitution (S_N2) and proton transfer (PT) channels at different collision energies leading to NH_2F + Cl^- and HF + $NHCl^-$ products, respectively.

6.2 kcal mol^{-1} for proton transfer, and this reaction channel is not observed at a lower collision energy corresponding to 300 K (~0.9 kcal mol^{-1}), in agreement with experiment,[25] but opens at an E_{coll} value of 40 kcal mol^{-1}. P_r in Fig. 2 shows that it prevails over the substitution channel (S_N2) at small b values, but becomes less preferred for the larger b values, although both reactions extend to the similarly large b_{max} value of ~5 Å. Accordingly, the reaction cross section of the PT pathway (3.0 ± 0.6 Å^2) is around one-half that of the S_N2 pathway (5.3 ± 1.3 Å^2); thus, proton transfer contributes ~36% of the reaction at this collision energy. The importance of proton transfer is expected to increase with E_{coll} and may surpass the S_N2 reaction channel at high E_{coll}.[21,37–39]

The reaction rate constant of $k(E_{coll}, T_v, T_r) = v(E_{coll})\sigma(E_{coll}, T_v, T_r)$ is estimated from the calculated cross section. For the simulations at 300 K only S_N2 products $NH_2F + Cl^-$ are formed, and σ for their formation gives a rate constant of $(7.8 \pm 0.8) \times 10^{-10}$ cm^3 mol^{-1} s^{-1}. The $F^- + NH_2Cl$ reaction becomes slower at E_{coll} = 40 kcal mol^{-1}, where both the S_N2 $NH_2F + Cl^-$ and proton transfer $HF + NHCl^-$ products are formed in the simulations, and the obtained rate constant based on the total σ for their formation is ~(4.1 ± 0.9) × 10^{-10} cm^3 mol^{-1} s^{-1}. This finding is in accordance with the negative temperature or E_{coll} dependence of the reactivity that has been shown experimentally and has been predicted theoretically for the C-center S_N2 reactions.[5,11,15,16] The rate constant has been measured for loss of F^- by a reaction with NH_2Cl at room temperature and is approximately (28.5 ± 14.3) × 10^{-10} cm^3 mol^{-1} s^{-1}.[25] Taking the statistical uncertainty in experiment into account, the trajectory rate constant at 300 K approaches the lower bound of the measured value, and the difference in the two sets of rate constants is discussed in the section of comparison between reactions of F^- with NH_2Cl and CH_3Cl.

Atomistic reaction mechanisms

Different types of reaction mechanisms are identified by animating trajectories and determining their atomic-level motions. S_N2 reaction $F^- + NH_2Cl \rightarrow NH_2F + Cl^-$ occurs by direct rebound, direct stripping, as well as indirect mechanisms. Rebound is a small impact parameter event, for which F^- directly attacks the backside of NH_2Cl, rebounds backward off the massive Cl-atom, and forms an excited N–F bond in the NH_2F molecule. This is a classical S_N2 path with Walden inversion that can be found in organic chemistry textbooks. Stripping occurs at larger b values, where F^- approaches the side of the chloramine molecule and strips the NH_2 group away from the Cl-atom, with NH_2F scattering in the forward direction. The indirect reaction is more complicated and occurs by multiple mechanisms including roundabout (RA), formation of the pre-reaction complex F^-–HNHCl (A) or post-reaction complex FNH_2–Cl^- (B), proton exchange (PE), central barrier recrossing (br), and combinations of these processes. Roundabout was reported for the C-center $F^-/Cl^- + CH_3I$ S_N2 reactions,[27,40] and for this mechanism F^- strikes the NH_2 group on its side, causing it to rotate around the massive Cl-atom. Then after one or more NH_2 revolutions, F^- attacks the N-atom backside and directly displaces Cl^-. Complex formation means the F^-–HNHCl and/or FNH_2–Cl^- complexes have multiple vibrations between the anion and the molecular moiety, resulting in a lifetime that is observable in the atomic animations. For the proton exchange between the F^-–HNHCl and FH–$NHCl^-$ complexes, the loss and gain of a proton by F^- occurs one or several times before S_N2 substitution and this mechanism occurs always coupled with the pre-reaction complex A formation. Barrier recrossing, initially observed in the $Cl^- + CH_3Cl$ central barrier dynamics[41] and also reported for the $F^- + CH_3F$ collisions,[37] recurred for the current N-center S_N2 reaction. The indirect trajectory covers a broad impact parameter range up to b_{max}, and long time retention in the intermediate region allows extensive overall rotation of the system, randomizing the scattering distributions.

Fractions of different S_N2 atomistic mechanisms are compared in Fig. 3, and their relative importance depends on the collision energy. Overall, the indirect reaction prevails, contributing 70–90% of the $F^- + NH_2Cl \rightarrow NH_2F + Cl^-$ S_N2 reaction at different E_{coll}, even if more direct processes are seen at a high energy. The direct reaction evolves from a rebound-stripping balanced distribution at 300 K towards more stripping events at a higher E_{coll} value of 40 kcal mol^{-1}. At both collision energies, the indirect reaction features a complex-mediated dynamics, in which the reactants are usually trapped in the entrance channel forming a hydrogen-bonded F^-–HNHCl complex and this complex is involved in almost all of the reactive trajectories

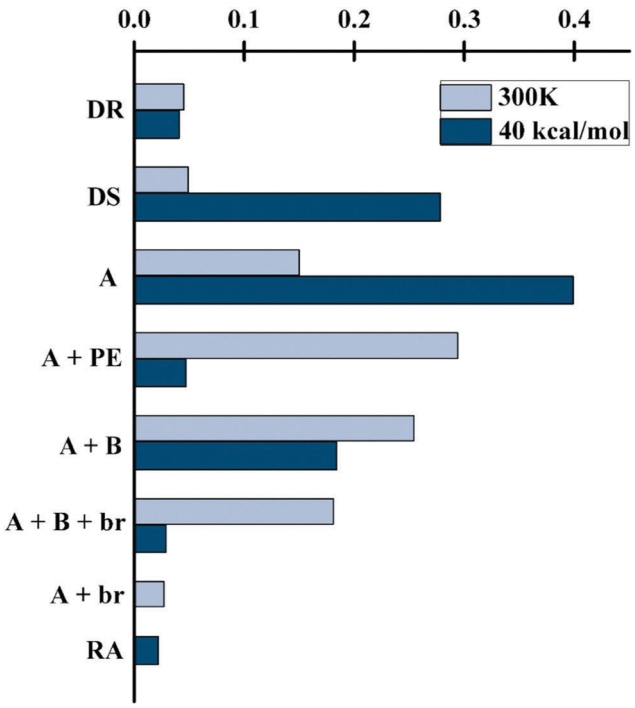

Fig. 3 Branching ratios of the atomistic reaction mechanisms for the $F^- + NH_2Cl \rightarrow NH_2F + Cl^-$ S_N2 reaction at different collision energies. DR and DS are direct pathways denoting rebound and stripping. Others are indirect events where the individual dynamics are characterized by (A) F^-–HNHCl; (B) FNH_2–Cl^-; PE, proton exchange; br, barrier recrossing; and RA, roundabout, respectively.

that proceed through an indirect pathway. Complex formation in the product exit channel is found to play a less important role in the high energy dynamics, but becomes pronounced as E_{coll} is lowered to 300 K, where its possibility taking part in the reaction increases to ~40%, resulting from the slow separation of the product species. This is the case for proton exchange and barrier recrossing as well and at 300 K the indirect events with participation of the two mechanisms contribute approximately 30 and 20% to the overall S_N2 reaction, respectively. In line with a finding for the C-center $Cl^- + CH_3I$ reaction[27] that large collision energy favors the roundabout mechanism, this interesting indirect event is observed only at E_{coll} = 40 kcal mol^{-1}, but found insignificant in the dynamics and accounts for ~2% of the reactive trajectories. Atomistic snapshots illustrating the direct rebound and stripping and an indirect mechanism, with entrance-channel complex formation that dominates the $F^- + NH_2Cl$ S_N2 reaction, are depicted in Fig. 4.

The $F^- + NH_2Cl \rightarrow HF + NHCl^-$ proton transfer channel becomes available at a greater E_{coll} value of 40 kcal mol^{-1}. As for the S_N2 pathway, the simulations reveal that this reaction also occurs by the direct rebound, direct stripping, and an indirect mechanism in which the formation of the F^-–HNHCl complex is important. The probabilities of these mechanisms are depicted in Fig. S1 in the ESI,† where it is seen that the proton transfer reaction is governed by direct stripping rather than the indirect events, in contrast to the S_N2 reaction. This dominant stripping mechanism, as shown in Fig. S2 (ESI†), was also found in the C-center $X^- + CH_3I \rightarrow HX + CH_2I^-$ (X = F and OH) proton transfer reactions.[38,39] Recently, Szabó and Czakó identified rebound and stripping as the direct mechanisms of the proton abstraction as well in $F^- + CHD_2Cl$. Interestingly, by distinguishing between back-side and front-side attacks, they further revealed three different direct abstraction pathways, namely, back-side rebound, back-side stripping, and front-side stripping, gaining deeper insight into the mechanisms of the abstraction process.[42]

Comparison with $F^- + CH_3Cl$ dynamics and central atom effects

The $F^- + CH_3Cl$ PES profile has been characterized using a high level focal-point analysis (FPA) approach,[21] which is compared with that of the current $F^- + NH_2Cl$ reaction in Fig. 1. There exist S_N2 and proton transfer product channels for both reactions.

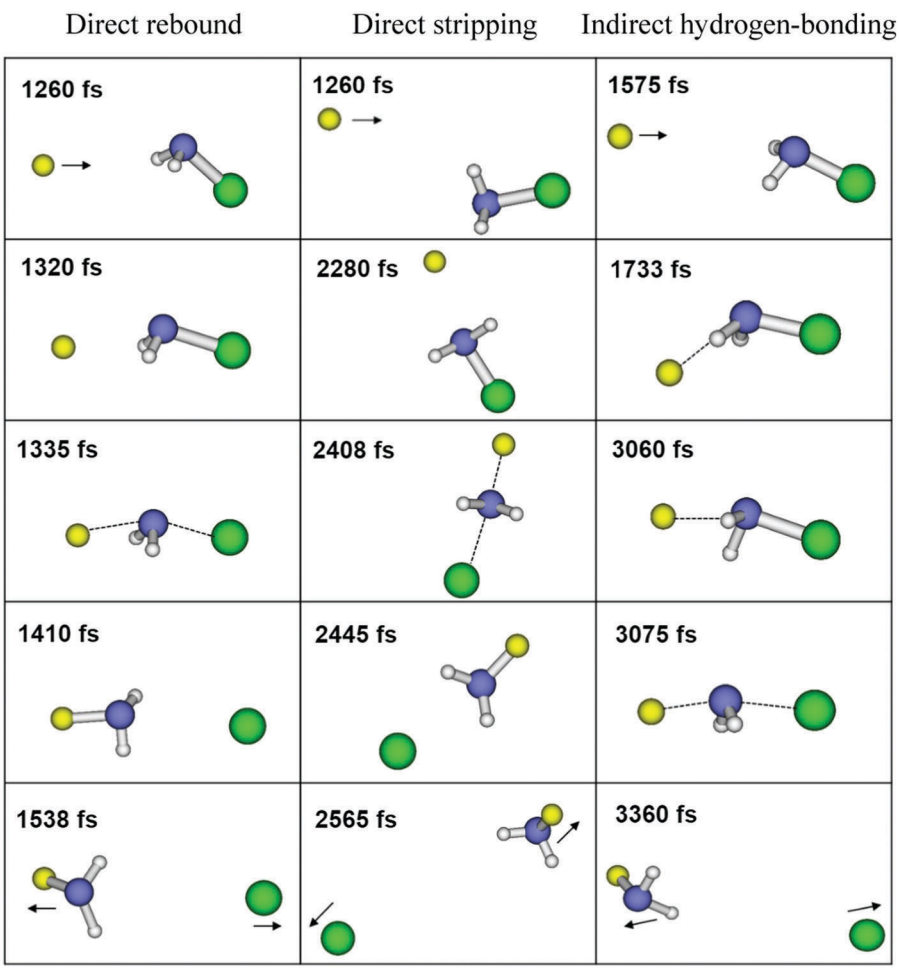

Fig. 4 Atomistic dynamics of representative trajectories illustrating the direct rebound and stripping events, and a dominant indirect mechanism of the $F^- + NH_2Cl \rightarrow NH_2F + Cl^-$ S_N2 reaction. The indirect trajectory proceeds through formation of a hydrogen-bonded F^-–HNHCl complex in the reactant entrance channel.

The MEP for S_N2 lies submerged with respect to the reactant asymptote and generally exhibits a double-well potential model, the one well known for S_N2@C.[2,12] Nevertheless, as opposed to the ion–dipole complexes F^-–CH_3Cl and FCH_3–Cl^- of co-linear C_{3v} symmetry, the corresponding nitrogen species F^-–HNHCl and FNH_2–Cl^- on both sides of the reaction central barrier lose all symmetry and are characterized by a NH–X (X = F or Cl) hydrogen bond. Moreover, besides the F^-–CH_3Cl complex, a second close-lying hydrogen-bonded complex of C_s symmetry (F^-–HCH_2Cl) is found as a minimum energy structure in the F^- + CH_3Cl entrance channel and these complexes can transform into each other readily, as expected based on the small barrier between them. In going from F^- + CH_3Cl to F^- + NH_2Cl, the S_N2 reaction becomes less exothermic (−31.9 *vs.* −17.0 kcal mol^{-1}), whereas the central barrier from the hydrogen-bonded F^-–HCH_2Cl/F^-–HNHCl pre-reaction complex to the corresponding S_N2 transition state is enhanced by ∼6 kcal mol^{-1}.

The proton transfer pathway shows a close resemblance for both CH_3Cl and NH_2Cl reactions, and shares the same F^-–HCH_2Cl/F^-–HNHCl hydrogen-bonded entrance channel complex with the S_N2 pathway in proceeding from the reactants to products. Nonetheless, when F^- reacts with NH_2Cl instead of CH_3Cl, the PT pathway decreases essentially in energy (Fig. 1), which suggests the H-abstraction at nitrogen might be energetically more facile than at carbon.

The F^- + CH_3Cl reaction has been explored utilizing the FA-SIFT technique[43] and QCT calculations.[5,21] It is of interest to compare it with the F^- + NH_2Cl reaction studied here, accordingly probing the central atom effects on S_N2 dynamics. A good agreement has been found in the F^- + CH_3Cl rate constant between the experiment and simulations, which give the respective values of $(14.1 \pm 0.1) \times 10^{-10}$ and 18.1×10^{-10} cm^3 mol^{-1} s^{-1} at 300 K. As shown in the reactivity section, the corresponding rates for the NH_2Cl reaction[25] are $(28.5 \pm 14.3) \times 10^{-10}$ and $(7.8 \pm 0.8) \times 10^{-10}$ cm^3 mol^{-1} s^{-1}, respectively. At 300 K, simulations in line with experiment show that only the S_N2 channel opens for both reactions. The opacity function from the trajectory reveals that CH_3Cl $P_r(b)$ is overall larger than that of NH_2Cl and, in addition, $P_r(b)$ extends to ∼14 Å for CH_3Cl but only to ∼12 Å for NH_2Cl.[5] As a result, the cross-section σ for CH_3Cl is higher than the NH_2Cl value, which leads to a larger CH_3Cl reaction rate in trajectory calculations in view of the almost same relative velocity $v(E_{coll})$ of reactants at 300 K for the two systems. For the NH_2Cl reaction, the lower simulation rate, as compared to the experiment, probably has multiple origins. As discussed above, an important factor would arise from a maximum impact parameter b_{max} and/or opacity function $P_r(b)$ given by B3LYP which is smaller. In the future, it is of significance to further test additional electronic structure theories and determine which one, and its PES properties, gives accurate dynamics for the F^- + NH_2Cl → NH_2F + Cl^- S_N2 reaction at different collision energies. A better resolution of the experimental rate constant is desirable as well, which would be of benefit for confirming the accuracy of the simulations.

The rate constant for F^- + CH_3Cl has been measured for E_{coll} from ∼0.5 to 23.1 kcal mol^{-1} and a T_{vr} value of ∼300 K,[44] with a value of 15.0×10^{-10} cm^3 mol^{-1} s^{-1} at E_{coll} = 0.9 kcal mol^{-1}, the average collision energy at 300 K temperature, in agreement with the FA-SIFT result of $(14.1 \pm 0.1) \times 10^{-10}$ cm^3 mol^{-1} s^{-1} for reactants at a 300 K thermal energy.[43] Considering the extrapolation of the constant for higher energy, the experimental rate for F^- + CH_3Cl at E_{coll} = 40 kcal mol^{-1} is approximated as 0.8×10^{-10} cm^3 mol^{-1} s^{-1}, which compares well with a simulation value of 0.9×10^{-10} cm^3 mol^{-1} s^{-1} in terms of a reaction cross-section (1.8 Å^2) from QCT computations.[21] Thus, raising E_{coll} from that corresponding to 300 K (∼0.9 kcal mol^{-1}) to 40 kcal mol^{-1} implies a drop in reactivity of a factor of ∼18–20 (*vide supra*). Though an experimental rate constant at 40 kcal mol^{-1} has not been reported for F^- + NH_2Cl, as shown in the reactivity section, trajectory calculations give a value of $(4.1 \pm 0.9) \times 10^{-10}$ cm^3 mol^{-1} s^{-1}, which is only about one-half of the simulation rate of $(7.8 \pm 0.8) \times 10^{-10}$ cm^3 mol^{-1} s^{-1} at 300 K. It is seen that both NH_2Cl and CH_3Cl reactions show the negative E_{coll} dependence of the reactivity. This is understood that the two reactions are governed by the S_N2 mechanism and for an exothermic S_N2 reaction with no overall barriers (see Fig. 1), collision energy inhibits the reaction. Nonetheless, going from NH_2Cl to CH_3Cl accentuates the negative E_{coll} dependence, and it is qualified by the more reduced reaction cross-section (8.3 *vs.* 1.8 Å^2) for the latter at a higher E_{coll} value of 40 kcal mol^{-1}.[21]

Note that the proton transfer pathway is open at E_{coll} = 40 kcal mol^{-1} for both reactions. Using QCT propagations, Czakó *et al.* estimated the branching ratio between S_N2 and PT for the F^- + CH_3Cl reaction, and the resulting value is around 0.67 : 0.33 at this energy.[21] With respect to F^- + CH_3Cl, the PT pathway becomes energetically more preferred in the nitrogen analogue F^- + NH_2Cl (Fig. 1). Interestingly, this feature for the reaction energetics does not manifest itself in the dynamics at a 40 kcal mol^{-1} collision energy and the present trajectory simulations for the NH_2Cl reaction parallel the QCT studies of the CH_3Cl reaction giving a SN/PT ratio of 0.64 : 0.36. The results suggest that the MEPs between stationary points are just signatures of the PES, and may only make minor contributions to the dynamics for the high energy 40 kcal mol^{-1} reaction.

Direct rebound, direct stripping, and indirect atomistic pathways are identified for both F^- + CH_3Cl → CH_3F + Cl^-[5,21,24] and F^- + NH_2Cl → NH_2F + Cl^- S_N2 dynamics, but the two reactions differ in their relative contributions when varying the collision energy. At a low E_{coll} value of ∼1 kcal mol^{-1}, the indirect events govern both reactions, in which the pre-reaction complex plays major roles. The dominant mechanism shifts from indirect to direct rebound for CH_3Cl upon raising the E_{coll} value to around 30–45 kcal mol^{-1}, but remains unchanged for NH_2Cl at E_{coll} = 40 kcal mol^{-1} despite more stripping trajectories observed here. Thus, the indirect probability is promoted for the NH_2Cl reaction. An important interaction potential in the entrance channel may be partly responsible for the observed mechanism difference, which is modified by the central atom to essentially change the overall energetics and also the underlying dynamics. A difference in the interaction potential is seen from the stability of the nucleophile F^- attachment to the substrate. As shown in

Fig. 1, the hydrogen-bonded F^-–HNHCl complex is bound by ~30 kcal mol^{-1}, while F^-–HCH_2Cl is bound by only 17 kcal mol^{-1}, which deepens the entrance well of the NH_2Cl reaction with respect to both the reactants and displacement saddle point and is assumed to help stabilizing the pre-reactive S_N2 intermediates. This may consequently enhance the indirect mechanism for F^- + NH_2Cl, even at an initially larger collision energy, with reactants transiently trapped in the pre-reaction potential energy well. A correlation of the reactant interaction with the atomistic mechanism was also found by Wester and co-authors in the reaction of F^- with methyl halides.[24] Because of the disparity between the low frequency intermolecular modes and the higher frequency intramolecular modes of the F^-–HNHCl complex, there exists a bottleneck in attaining the S_N2 transition state, as predicted in previous studies for the Cl^-–CH_3Cl and Cl^-–CH_3Br pre-reaction complexes,[45] which as well contributes to a large fraction of the F^- + NH_2Cl reaction that occurs indirectly at a high collision energy of 40 kcal mol^{-1}.

At E_{coll} = 40 kcal mol^{-1}, direct stripping events dominate the proton transfer channel in the F^- + NH_2Cl reaction, regardless of the presence of a hydrogen-bonded entrance channel complex, but become not significant for that in the F^- + CH_3Cl reaction, attributed to its lowered PT reaction cross-section.[21] Interestingly, the reaction of CH_3I with F^- at a E_{coll} value of ~35 kcal mol^{-1} resembles the present reaction of NH_2Cl, which features the dominant direct stripping mechanism for the proton transfer dynamics as well.[39]

The energy partitioning and scattering angle distributions of the reaction products, which are experimentally measurable, usually assist in probing the atomic-level mechanisms of a chemical reaction. These results are reported for the F^- + NH_2Cl → NH_2F + Cl^- S_N2 reaction in Table S1 and Fig. S3 in the ESI.† In general, the product energy is mainly partitioned to the relative translation for direct rebound and stripping trajectories, especially at higher collision energy, but to the internal degrees of freedom for the indirect trajectories, in accord with those predicted for the C-center S_N2 reactions.[5,24,27,38–40,46] For indirect reactions ~70–80% of the internal energy goes to the product vibration with less contributions to the rotation. At a low E_{coll} value corresponding to 300 K (~0.9 kcal mol^{-1}), the overall product internal excitation with a fraction of 0.72 ± 0.02 is significantly hotter than the translational energy, since at 300 K the indirect mechanism dominates, which minimizes the kinetic energy release and most of the available energy transfers into vibrations, in agreement with the results for the F^- + CH_3Cl → CH_3F + Cl^- reaction at similar E_{coll} = 1 kcal mol^{-1}.[5] The principal mechanism remains indirect for NH_2Cl at E_{coll} = 40 kcal mol^{-1}, but changes to direct rebound events for CH_3Cl at an E_{coll} value in the range of 30–45 kcal mol^{-1},[21,24] as described above. Consequently, the larger internal energy faction (0.58 ± 0.03) is still seen at a higher E_{coll} value for the NH_2Cl reaction, irrespective of the enlarged partitioning to translation arising from the enhanced direct stripping contributions. In contrast, here most of the excess collision energy transfers into the relative translation energy of the products for the CH_3Cl reaction, as found in both ion-imaging experiments and QCT computations.[21,24]

The velocity scattering angle distributions of the NH_2Cl and CH_3Cl[5,21,24] reactions show qualitatively the same features for the direct events at both collision energies. As seen in Fig. S3 (ESI†), the scattering is primarily backward for the rebound mechanism within a cos(θ) range of −1.0–0, whereas the stripping trajectories display forward scattering with cos(θ) between 0 and 1.0. The indirect scattering occurs at every direction. For 300 K (E_{coll} ~ 0.9 kcal mol^{-1}), this scattering is anisotropic, with a peak at backward directions (cos(θ) close to −1.0) and a more substantial peak at forward directions (cos(θ) close to 1.0). The large contribution of indirect mechanisms at 300 K also gives rise to a similar shape for the overall scattering angle distributions of the NH_2Cl reaction, resembling that of the corresponding CH_3Cl reaction at E_{coll} = 1 kcal mol^{-1} (Fig. 5 in ref. 5). The indirect trajectory shows a forward-backward balanced distribution at 40 kcal mol^{-1}. Here, a sum of rebound, stripping, and indirect mechanisms causes an isotropic scattering of the total NH_2Cl reaction, as compared to a backward-dominated distribution for the CH_3Cl scattering at 30–45 kcal mol^{-1}, ascribed to the prominent direct rebound events.[21,24] The observed disagreement in the angular distributions for a higher E_{coll} value could therefore be explained by a difference in the branching ratios for the backward-scattered rebound, the forward-scattered stripping, and the indirect mechanisms in the NH_2Cl reaction in contrast to the C-center CH_3Cl.

Conclusions

The direct dynamics simulations offer an efficient approach to investigate the atomic-level mechanisms for the N-center F^- + NH_2Cl S_N2 reaction and compare with the C-center F^- + CH_3Cl congener,[5,21,24] thereby gaining insight into the role the central atom might play in the underlying reaction dynamics. Both the substitution (S_N2) and proton transfer (PT) product channels are observed from the trajectory propagations for the two reactions and S_N2 is found to dominate independent of E_{coll} due to its more favored reaction energetics. The proton transfer channel opens at a higher collision energy and although it becomes more submerged with respect to the reactant asymptote in going from CH_3Cl to NH_2Cl, trajectory simulations at E_{coll} = 40 kcal mol^{-1} predict a similar branching ratio of S_N2/PT for both reactions, suggesting that this characteristic does not manifest itself in the high energy dynamics.

Both CH_3Cl and NH_2Cl S_N2 MEPs have a double-well potential model and feature a hydrogen-bonded F^-–HCH_2Cl/F^-–HNHCl complex in the reactant entrance channel. Overall, the pre-reaction complex is found to play a decisive role in the F^- + NH_2Cl/CH_3Cl substitution dynamics even though more weights are seen for the post-collision interaction at a 300 K thermal energy in the NH_2Cl case, attributed to the small energy release in the exit channel contributing to the product species separation. As established for S_N2@C,[1,16,38] the F^- + CH_3Cl reaction exhibits an indirect scattering *via* a F^-–HCH_2Cl/F^-–CH_3Cl pre-reaction

complex at low energy, transitioning to the direct rebound events that visualize S_N2-reactions in organic chemistry text books, as reactive encounters carry more kinetic energy. In contrast, altering the central atom from carbon to nitrogen introduces subtle changes in the interaction potential of the approaching reactants leading to the indirect pathway that prevails for the F^- + NH_2Cl S_N2 reaction, even at high energy. This indirect dynamics are governed by forming a reaction intermediate in the hydrogen-bonded F^-–HNHCl pre-reaction potential energy well. A larger fraction of the indirect mechanism at a higher E_{coll} value may also be a consequence of the inefficient energy transfer from the intermolecular modes of the F^-–HNHCl complex to the N–Cl stretch[45] and in future work, it will be of interest to investigate the coupling between these modes. Inspecting the angular and energy distributions reveals that the F^- + NH_2Cl S_N2 reaction produces internally hot product molecules with distinct scattering features at different collision energies, which may be well correlated with a variation in the relative contributions of the multiple atomistic reaction mechanisms and would stimulate further examinations in experiment.

The present findings show that compared to the well-studied S_N2@C, the dynamics of S_N2@N are quite complicated and much different, for which an indirect complex-mediated mechanism is of significance. The simulations further find that the roundabout mechanism[27] may participate in the N-center S_N2 dynamics at high collision energy. Together with the recently discovered roaming[26] and novel double inversion[21] mechanisms, indirect reaction dynamics are thus found to be much more important, for S_N2 as well as other and more complex ion–molecule reactions, than currently anticipated. The results highlight the fundamental role of the central atom, in addition to the nucleophile and the leaving group, not only for S_N2 reactivity but the underlying reaction dynamics. Further studies are underway to explore other and more complex S_N2@N systems as well as the effects of different central atoms and consider additional quantum chemical theories for the direct dynamics, which will enrich our understanding of these fundamental nucleophilic substitution mechanisms with a different reaction center.

Acknowledgements

This work is supported by the National Natural Science Foundation of China (no. 21573052, 21403047, 51536002), the Fundamental Research Funds for the Central Universities, China (AUGA5710012114, 5710012014), the Natural Science Foundation of Heilongjiang Province of China (no. B2017003), the SRF for ROCS, SEM, China, and the Open Project of Beijing National Laboratory for Molecular Sciences (no. 20140103, 20150158). Support is also provided by the High Performance Computing Center (HPCC) at Texas Tech University, under the direction of Philip W. Smith.

References

1 J. Xie and W. L. Hase, *Science*, 2016, **352**, 32–33.
2 M. L. Chabinyc, S. L. Craig, C. K. Regan and J. I. Brauman, *Science*, 1998, **279**, 1882–1886.
3 J. Xie, R. Sun, M. R. Siebert, R. Otto, R. Wester and W. L. Hase, *J. Phys. Chem. A*, 2013, **117**, 7162–7178.
4 L. Sun, K. Song and W. L. Hase, *Science*, 2002, **296**, 875–878.
5 I. Szabó, A. G. Csaszar and G. Czako, *Chem. Sci.*, 2013, **4**, 4362–4370.
6 R. Sun, C. J. Davda, J. X. Zhang and W. L. Hase, *Phys. Chem. Chem. Phys.*, 2015, **17**, 2589–2597.
7 P. Beak and J. Li, *J. Am. Chem. Soc.*, 1991, **113**, 2796–2797.
8 M. Bühl and H. F. Schaefer III, *J. Am. Chem. Soc.*, 1993, **115**, 9143–9147.
9 Y. Y. Liu, S. J. Ren, J. Huang, Y. T. Liang, X. G. Wei, Y. Ren, K. C. Lau and J. Zhu, *Curr. Org. Chem.*, 2016, **20**, 1058–1068.
10 I. Fernández and F. M. Bickelhaupt, *Chem. Soc. Rev.*, 2014, **43**, 4953–4967.
11 J. K. Laerdahl and E. Uggerud, *Int. J. Mass Spectrom.*, 2002, **214**, 277–314.
12 Y. Wang, H. W. Song, I. Szabó, G. Czakó, H. Guo and M. H. Yang, *J. Phys. Chem. Lett.*, 2016, **7**, 3322–3327.
13 W. P. Hu and D. G. Truhlar, *J. Am. Chem. Soc.*, 1995, **117**, 10726–10734.
14 M. N. Glukhovtsev, A. Pross and L. Radom, *J. Am. Chem. Soc.*, 1996, **118**, 6273–6284.
15 A. A. Viggiano, R. A. Morris, J. S. Paschkewitz and J. F. Paulson, *J. Am. Chem. Soc.*, 1992, **114**, 10477–10482.
16 P. Manikandan, J. X. Zhang and W. L. Hase, *J. Phys. Chem. A*, 2012, **116**, 3061–3080.
17 J. Lv, J. X. Zhang and D. Y. Wang, *Phys. Chem. Chem. Phys.*, 2016, **18**, 6146–6152.
18 D. P. Geerke, S. Thiel, W. Thiel and W. F. van Gunsteren, *J. Chem. Theory Comput.*, 2007, **3**, 1499–1509.
19 Y. Feng, *J. Comput. Chem.*, 2012, **33**, 401–405.
20 M. A. F. de Souza, T. C. Correra, J. M. Riveros and R. L. Longo, *J. Am. Chem. Soc.*, 2012, **134**, 19004–19010.
21 I. Szabó and G. Czakó, *Nat. Commun.*, 2015, **6**, 5972.
22 I. Szabó, B. Olasz and G. Czakó, *J. Phys. Chem. Lett.*, 2017, **8**, 2917–2923.
23 X. Liu, J. X. Zhang, L. Yang and R. Sun, *J. Phys. Chem. A*, 2016, **120**, 3740–3746.
24 M. Stei, E. Carrascosa, M. A. Kainz, A. H. Kelkar, J. Meyer, I. Szabó, G. Czakó and R. Wester, *Nat. Chem.*, 2016, **8**, 151–156.
25 R. Gareyev, S. Kato and V. M. Bierbaum, *J. Am. Soc. Mass Spectrom.*, 2001, **12**, 139–143.
26 D. Townsend, S. A. Lahankar, S. K. Lee, S. D. Chambreau, A. G. Suits, X. Zhang, J. Rheinecker, L. B. Harding and J. M. Bowman, *Science*, 2004, **306**, 1158–1161.
27 J. Mikosch, S. Trippel, C. Eichhorn, R. Otto, U. Lourderaj, J. X. Zhang, W. L. Hase, M. Weidemüller and R. Wester, *Science*, 2008, **319**, 183–186.
28 X. U. Hu, W. L. Hase and T. Pirraglia, *J. Comput. Chem.*, 1991, **12**, 1014–1024.
29 U. Lourderaj, R. Sun, S. C. Kohale, G. L. Barnes, W. A. de Jong, T. L. Windus and W. L. Hase, *Comput. Phys. Commun.*, 2014, **185**, 1074–1080.
30 M. Valiev, E. J. Bylaska, N. Govind, K. Kowalski, T. P. Straatsma, H. J. J. van Dam, D. Wang, J. Nieplocha,

E. Apra, T. L. Windus and W. A. de Jong, *Comput. Phys. Commun.*, 2010, **181**, 1477–1489.
31 G. H. Peslherbe, H. B. Wang and W. L. Hase, *Adv. Chem. Phys.*, 1999, **105**, 171–202.
32 M. J. Ryding, A. Debnárová, I. Fernández and E. Uggerud, *J. Org. Chem.*, 2015, **80**, 6133–6142.
33 J. G. López, G. Vayner, U. Lourderaj, S. V. Addepalli, S. Kato, W. A. deJong, T. L. Windus and W. L. Hase, *J. Am. Chem. Soc.*, 2007, **129**, 9976–9985.
34 J. X. Zhang, L. Yang, J. Xie and W. L. Hase, *J. Phys. Chem. Lett.*, 2016, **7**, 660–665.
35 M. R. Siebert, J. X. Zhang, S. V. Addepalli, D. J. Tantillo and W. L. Hase, *J. Am. Chem. Soc.*, 2011, **133**, 8335–8343.
36 J. A. Montgomery, M. J. Frisch, J. W. Ochterski and G. A. Petersson, *J. Chem. Phys.*, 2000, **112**, 6532–6542.
37 I. Szabó, H. Telekes and G. Czakó, *J. Chem. Phys.*, 2015, **142**, 244301.
38 J. Xie, R. Sun, M. R. Siebert, R. Otto, R. Wester and W. L. Hase, *J. Phys. Chem. A*, 2013, **117**, 7162–7178.
39 J. X. Zhang, J. Xie and W. L. Hase, *J. Phys. Chem. A*, 2015, **119**, 12517–12525.
40 J. Mikosch, J. X. Zhang, S. Trippel, C. Eichhorn, R. Otto, R. Sun, W. A. de Jong, M. Weidemüller, W. L. Hase and R. Wester, *J. Am. Chem. Soc.*, 2013, **135**, 4250–4259.
41 Y. J. Cho, S. R. Vande Linde, L. Zhu and W. L. Hase, *J. Chem. Phys.*, 1992, **96**, 8275–8287.
42 I. Szabó and G. Czakó, *J. Chem. Phys.*, 2016, **145**, 134303.
43 R. A. J. O'Hair, G. E. Davico, J. Hacaloglu, T. T. Dang, C. H. DePuy and V. M. Bierbaum, *J. Am. Chem. Soc.*, 1994, **116**, 3609–3610.
44 T. Su, R. A. Morris, A. A. Viggiano and J. F. Paulson, *J. Phys. Chem.*, 1990, **94**, 8426–8430.
45 W. L. Hase, *Science*, 1994, **266**, 998–1002.
46 B. Olasz, I. Szabó and G. Czakó, *Chem. Sci.*, 2017, **8**, 3164.